Forschungszentrum Karlsruhe

Technik und Umwelt

Wissenschaftliche Berichte

FZKA 6354

Numerical Simulations of Buoyant Magnetohydrodynamic Flows Using the CFX Code

I. Di Piazza, L. Bühler

Institut für Kern- und Energietechnik
Projekt Kernfusion

Forschungszentrum Karlsruhe GmbH, Karlsruhe
1999

Numerical simulations of buoyant magnetohydrodynamic flows using the CFX code

Abstract

The buoyancy-driven magnetoconvection in a vertical square duct is investigated numerically using the CFX package. The implementation of an MHD problem in CFX is discussed, with particular reference to the Lorentz forces and electric potential boundary conditions for arbitrary electrical conductivity of the walls. The method proposed is general, and applies to arbitrary geometries with an arbitrary orientation of the magnetic field. Results for fully developed flow under various thermal boundary conditions are compared with asymptotic analytical solutions. The comparison shows that, for higher values of the wall conductivity, the asymptotic analysis is confirmed, and high velocity jets occur at the side walls. For lower values, the side layers become better conducting than the side walls and high current jets appear parallel to the side walls. As a consequence, velocity jets don't occur anymore and the core solution is corrected just by viscous forces at the wall. The capability of CFX in describing properly an MHD problem is proved.

Numerische Simulation von magnetohydrodynamischen Konvektionsströmungen mit CFX

Zusammenfassung

Unter Verwendung des Programmpakets CFX werden schwerkraftgetriebene Konvektionsströmungen in Magnetfeldern untersucht. Am Beispiel der Lorentz Kräfte und der elektrischen Randbedingungen für beliebig elektrisch leitende Wände wird die Implementierung des Problems in CFX diskutiert. Die vorgeschlagene Methode ist allgemein formuliert und kann für allgemeine Geometrien und beliebige Orientierung des Magnetfeldes angewandt werden. Ergebnisse für eingelaufene Strömungen mit unterschiedlichen thermischen Randbedingungen werden mit bekannten asymptotischen Lösungen verglichen. Der Vergleich zeigt eine gute Übereinstimmung für gut leitende Kanalwände. Die Geschwindigkeitsjets entlang von Seitenwänden werden korrekt berechnet. Für schlecht elektrisch leitende Wände konzentrieren sich elektrische Ströme in den dünnen Seitenschichten, Geschwindigkeitsjets verschwinden. Die Seitenschichten spielen dann eher eine passive Rolle und sorgen durch viskose Kräfte für einen Abbau der Geschwindigkeit in Wandnähe. Zusammenfassend wird gezeigt, daß es möglich ist, mit CFX MHD Probleme zu beschreiben.

Contents

1 Introduction

Two different schemes have been proposed in the last years for the liquid metal blankets of fusion reactors: in one of them the coolant coincides with the liquid metal itself (self-cooled concept), while in the other the heat flux is removed by separated coolant devices (i.e. water-cooled concept). A comparison of these two concepts is performed for example by Reimann, Benamati and Moreau (1996) within the European projects. In the self-cooled concept high velocities are required to remove heat; thus, the flow must be strongly forced, which is expressed by relatively large pressure losses induced by MHD effects. Under these conditions, the buoyancy effects are negligible. Of course, this is not the case for separated-cooled devices, where a weak forced flow is required only for tritium extraction, and relevant temperature gradients occur; therefore, the flow is mainly buoyancy driven.

Within this separately-cooled concept, the buoyant fully developed flow across a vertical square channel under the influence of a magnetic field, is investigated numerically. The walls are supposed to be electrically conducting and thin, and the influence of the wall conductivity on the flow pattern is studied. Various thermal conditions are examined: the differentially heated and the internally heated cases. The way how to implement an MHD problem for an arbitrary configuration in CFX is shown, with particular reference to the Lorentz forces, the potential equation, and the electrical boundary conditions.

For the same geometry, an asymptotic analysis has been developed by Bühler (1998) for large Hartmann numbers and well conducting walls parallel to the magnetic field, the so-called side walls. It will be shown that these analytical results are confirmed by numerical simulations for the higher conductivities of the wall; in particular, high velocity jets are correctly predicted in the side layers. For the lower values of wall conductivity, high current jets occur in the side layers, parallel to the side walls, and the numerical simulations show that velocity jets are no more present. Moreover, the capability of CFX in predicting actual MHD flows is proved.

In the past several authors solved numerically buoyant MHD flow problems Mößner and Gerbeth (1999) Ben Hadid and Henri (1997). Others like Mück (1998), Sterl (1990) solved pressure driven MHD flows. The common restrictions of all these analysis is that they are limited to very special geometries, hardly met in engineering piping systems. The use of CFX with the MHD modelling as proposed offers the possibility to perform inertial numerical simulations for relevant duct shapes and complex geometries.

2 Formulation

The problem presented here is the MHD buoyancy-driven flow in a vertical square duct. Fig.1 shows a sketch of the geometry. The magnetic field $\mathbf{B} = B\hat{\mathbf{y}}$ is parallel to one pair of the walls and orthogonal to the others. Walls normal to the magnetic field are called Hartmann walls. In the boundary layers close to these walls, the velocity profile is basically determined from a balance between Lorentz and viscous forces, and the thickness of these layers scales as $\delta_H \sim M^{-1}$, where M is the Hartmann number better defined later in the section. The walls parallel to the magnetic field direction are called side walls, and the boundary layers adjacent to these walls, the side layers. There thickness δ_s scales as $\delta_s \sim M^{-1/2}$. The temperature gradient is along $\hat{\mathbf{z}}$, and is supposed to be orthogonal with respect to the magnetic field direction $\hat{\mathbf{y}}$.

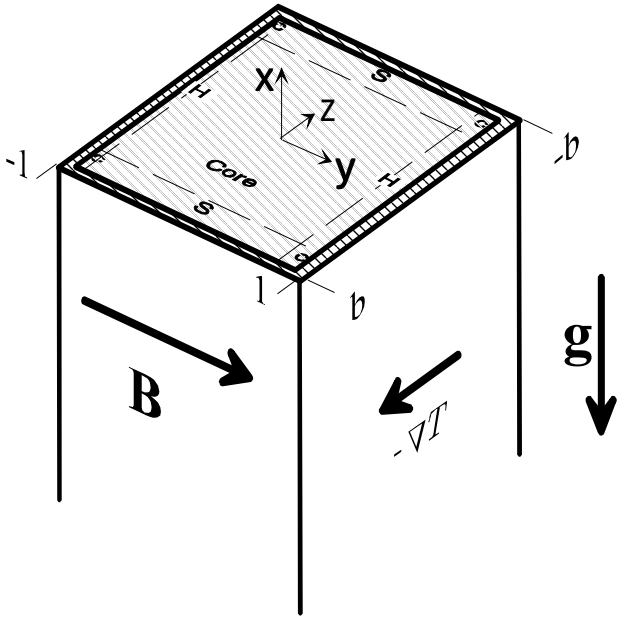

Figure 1: Sketch of the geometry of the channel. The gravity field is in the axis direction, and the magnetic field is parallel to one pair of walls and orthogonal to the others. The temperature gradient is in the $\hat{\mathbf{z}}$ diection, orthogonal to the magnetic field.

Under the assumption of a low magnetic Reynolds number, the induced magnetic field is negligible with respect to the applied field $\mathbf{B}$. Such an inductionless flow is governed by the momentum equation with the Boussinesq approximation for the buoyancy term,

$$\frac{Gr}{M^4}\left[\frac{\partial \mathbf{v}}{\partial t} + (\mathbf{v}\cdot\nabla)\,\mathbf{v}\right] = -\nabla p + \frac{1}{M^2}\nabla^2\mathbf{v} + \mathbf{j}\times\hat{\mathbf{y}} + T\hat{\mathbf{x}} \tag{1}$$

and the continuity equation,

$$\nabla\cdot\mathbf{v} = 0. \tag{2}$$

Gr is the Grashof number, which expresses the square of the ratio of buoyancy and viscous forces, defined as

$$Gr = g\beta\ \Delta T\ L^3/\nu^2, \tag{3}$$

where β is the thermal expansion coefficient of the fluid. The velocity vector $\mathbf{v} = (u, v, w)$ and the current density $\mathbf{j}$ are scaled respectively by $v_0 = \nu/L \cdot Gr/M^2$ and $j_0 = \sigma v_0 B$, where L is a characteristic length scale, ν is the kinematic viscosity and σ is the electrical conductivity of the fluid. The dimensionless pressure p is the difference between the local and the hydrostatic pressure, scaled by Lj_0B. The dimensionless temperature T is the difference between the temperature and a reference value T_0, scaled by a characteristic temperature difference ΔT. The square of the Hartmann number M is the ratio of electromagnetic to viscous forces, and can be defined as

$$M = LB\sqrt{\sigma/(\rho\nu)}, \tag{4}$$

where ρ is the density of the fluid.

These scales are particularly appropriate for strong magnetic fields, and one can observe that the velocity scale is the diffusion scale ν/L times the quantity Gr/M^2; this quantity is actually the ratio of buoyant to electromagnetic forces and keeps into account the damping effect of the magnetic field. The current is evaluated via Ohm's law

$$\mathbf{j} = -\nabla\phi + \mathbf{v} \times \hat{\mathbf{y}}, \tag{5}$$

together with the conservation of the electric charge

$$\nabla \cdot \mathbf{j} = 0. \tag{6}$$

The electrical potential ϕ is scaled by Lv_0B .

The temperature is governed by the energy balance

$$Pe\left[\frac{\partial \mathbf{v}}{\partial t} + (\mathbf{v} \cdot \nabla)\, T\right] = \nabla^2 T + Q \tag{7}$$

where Pe is the Péclet number $Pe = Pr \cdot Gr/M^2$, and Q represents the volumetric power density scaled by $\lambda \cdot \Delta T/L^2$, where λ is the thermal conductivity. Pr represents the Prandtl number defined as the ratio of kinematic viscosity and thermal diffusivity of the fluid.

The velocity boundary conditions are no-slip at the walls, while the thermal boundary conditions are $\mathbf{n} \cdot \nabla T = const.$ at the Hartmann walls, and $T = const.$ or $\mathbf{n} \cdot \nabla T = -q_w$ at the side walls, where $\mathbf{n}$ is the inward normal unity vector at the wall.

The electrical boundary condition is the thin wall condition Walker (1981)

$$\mathbf{j} \cdot \mathbf{n} = c_w \nabla_w^2 \phi \tag{8}$$

which expresses the conservation of the electric charge in the plane of the wall. The condition is integrated across the wall thickness and the constant c_w is called the wall conductance ratio $c_w = \sigma_w t$, where the conductivity of the wall is scaled by the fluid conductivity, and the dimensionless thickness of the wall t is assumed to be small $t << 1$.

For ducts long enough the flow is fully developed far from the ends; inertia doesn't play any role, and the left sides of Eqs. 1 and 7 vanish. Therefore, the solution is no more dependent on Gr and Pe, and the only relevant parameters entering the equations are M and c_w. The problem is actually two-dimensional in the plane perpendicular to the axis.

Under these conditions, an asymptotic analysis has been performed by Bühler (1998), with the further assumptions of large Hartmann number and wall conductivity of the side walls

$$c_s >> M^{-1/2}. \tag{9}$$

The latter condition actually means that the side walls must be much better conducting than the side layers, and therefore the currents are supposed to pass unchanged through the side layers and are completely closed through the walls.

3 Description of an MHD problem in CFX

CFX is a commercial package for fluid dynamic calculations, based on the Finite Volume technique and the SIMPLE family algorithms for the pressure-velocity coupling. It is, in principle, a very powerful and flexible code, for arbitrary geometries with orthogonal, polar, or body-fitted co-ordinates, turbulence models, chemical reactions, two-phase flow, etc..

Unlikely, MHD is not at all available as a simple option of the code features, and a magnetohydrodynamic problem must be properly described within the code. The equations describing the fluid behaviour in CFX can be summarised as: the momentum equation

$$\frac{\partial \bar{\rho}\bar{\mathbf{v}}}{\partial \bar{t}} + \bar{\rho}\left(\bar{\mathbf{v}}\cdot\nabla\right)\bar{\mathbf{v}} = -\nabla\bar{p} + \nabla\bar{\mu}\nabla\bar{\mathbf{v}} + S_m, \tag{10}$$

the continuity equation

$$\nabla\cdot\bar{\mathbf{v}} = 0, \tag{11}$$

the temperature equation

$$\frac{\partial \bar{\rho}\bar{c}_p\bar{T}}{\partial \bar{t}} + \nabla\cdot\left(\bar{\mathbf{v}}\bar{\rho}\bar{c}_p\bar{T}\right) = \nabla\bar{\lambda}\nabla\bar{T} + S_{\bar{T}}, \tag{12}$$

where the overbar is used to indicate the internal CFX variables. In addition, the transport of an arbitrary scalar is described by:

$$\frac{\partial \bar{\rho}\bar{\theta}}{\partial \bar{t}} + \nabla\cdot\left(\bar{\mathbf{v}}\bar{\rho}\bar{\theta}\right) = \nabla\bar{\Gamma_\theta}\nabla\bar{\theta} + S_{\bar{\theta}}. \tag{13}$$

In the following CFX will be applied to the non-dimensional problem (1-8). The coefficients with an overbar necessary for a CFX input are therefore chosen as

$$\bar{\rho} = \frac{Gr}{M^4}, \bar{\mu} = \frac{1}{M^2}, \bar{\lambda} = 1, \bar{c}_p = 1. \tag{14}$$

Such a choice allows an interpretation of the CFX-variables $\bar{\mathbf{v}}$, $\bar{p}$, $\bar{T}$, $\bar{\theta}$ as the dimensionless velocity vector $\mathbf{v}$, the pressure p, the electrical potential ϕ, and the temperature T, respectively. The reason why $\bar{T}$ is chosen to describe the electrical potential is, that Eq. 12 allows for more general boundary conditions than Eq. 13.

Basically, there are three points that have to be implemented in the external routines to the code.

The source term S_m in the Navier-Stokes equations includes buoyancy $\bar{\theta}\cdot\hat{\mathbf{x}}$ and Lorentz forces $\mathbf{j}\times\hat{\mathbf{y}}$. The Lorentz force term

$$\mathbf{j}\times\hat{\mathbf{y}} = -\nabla\phi\times\hat{\mathbf{y}} + \left(\mathbf{v}\times\hat{\mathbf{y}}\right)\times\hat{\mathbf{y}}, \tag{15}$$

can be split in the first part depending on the gradients of potential $-\nabla\phi\times\hat{\mathbf{y}}$, and a second part which is similar to a drag term $\left(\mathbf{v}\times\hat{\mathbf{y}}\right)\times\hat{\mathbf{y}} = -\mathbf{v}_\perp$ active in the plane perpendicular to the magnetic field. Therefore, the gradient of ϕ must be evaluated numerically across the domain, to determine the source term in the momentum equation.

From Eq. 5 and 6, an equation for the scalar electrical potential can be easily derived

$$-\nabla^2\phi = -(\nabla \times \mathbf{v}) \cdot \hat{\mathbf{y}} = S_{\bar{T}}. \tag{16}$$

Using this equation, the currents are eliminated from the problem. It can be recognized that Eq. 16 has the form of a purely diffusion transport equation, the source term being the component of vorticity along the magnetic field direction. Thus, it is possible to describe this equation in CFX as a scalar transport equation, with no convection, and a source term evaluated by the spatial derivatives of velocity.

From the electrical boundary conditions 8, it can be observed that inserting the Ohm's law 5, evaluated at the wall leads to

$$-\mathbf{n} \cdot \nabla\phi = c_w \nabla_w^2 \phi. \tag{17}$$

The potential equation 16 in the fluid, together with the boundary condition 17 is the electrical analogous to a heat transfer problem in a medium at rest, surrounded by a thin sheet of different conductivity. Such problems can be solved using existing routines in CFX in combination with the 'no convection' option, when the CFX-temperature $\bar{T}$ is interpreted as the electrical potential ϕ in the MHD problem under consideration. Then the CFX- heat fluxes represent simply the electric currents. This is valid at the walls, where the velocity vanishes and the currents becomes simply $\mathbf{j} = -\nabla\phi$. The CFX- heat fluxes in the fluid are, however, different from the current density because the physical problem there experiences in addition the induced electric field $\mathbf{v} \times \hat{\mathbf{y}}$.

As already pointed out Mück (1998), the Hartmann layer can be omitted in the model, integrating the equations analytically across the layer. As a result, at the Hartmann wall, the wall conductance ratio c_w must be replaced by $c_w + \delta_H$, where $\delta_H \sim M^{-1}$ is the total conductance of the layer. The physical model beyond this substitution is that the wall and the layer are electrical resistances in parallel. Eq. 17 is a Poisson equation with a source term originating from the normal gradients at the wall. To solve this equation, a direct Poisson solver was written, to get the value of the potential in the plane of the wall. The latter one is used as a Dirichelet boundary condition for the fluid domain. As already noticed Sterl (1990) in the case of forced MHD convection, within the global iterative procedure, the errors in evaluating potential derivatives at the wall are amplified by a factor of $1/c_w$. Therefore, convergence is more difficult to obtain for the lowest values of the wall conductance ratio c_w. To get converged calculations, a time-marching procedure has been used to couple the electrical boundary condition 17 with the solution inside the domain.

At the Hartmann walls, as already shown by Leboucher (1999), a reasonable condition for the tangential components of velocity, is the linear extrapolation from the values inside the domain. Such a condition is close to the free slip condition at the wall.

A more efficient way to describe an MHD problem in CFX, is to use only the internal solvers, already available within the code itself, also for the electrical boundary conditions. This is actually possible surrounding the whole fluid domain by a conducting solid wall of finite thickness t. Then the possibility is open to use the CFX heat transfer apparatus to find the electrical potential distribution. With this approach the correct boundary conditions are of zero 'flux' on the external faces of the solid walls: this ensures the global conservation of charge. It can be shown that, in Eq. 12 the convective

terms are not any more present in the solid regions, and stationary solutions become independent of $\bar{c}_p$ and $\bar{\rho}$ of the wall material and by setting properties for the solid walls as $\lambda_{side-wall} = 1/t \cdot c_w$, $\lambda_{Hartmann-wall} = 1/t \cdot (c_w + M^{-1})$, the thin wall condition expressed by 17 is satisfied for a converged solution. The latter method described is very general, because it applies to any geometry, described by body fitted coordinates, and thus it can be used for practical MHD configurations and complex devices, for which no self-made codes are available. The only point is to set the local physical properties for the solid wall in a proper way, for example

$$\lambda_{wall} = 1/t \cdot \left[(M \ \mathbf{n} \cdot \hat{\mathbf{y}})^{-1} + c_w \right], \tag{18}$$

where $\mathbf{n}$ is the normal unity vector to the wall and $\delta_H \sim (M \ \mathbf{n} \cdot \hat{\mathbf{y}})^{-1}$ is the local thickness of the Hartmann layer varying along the wall surface. The case of MHD fully developed duct flow of arbitrary cross section, magnetic field orthogonal to the axis, and conducting walls, has been studied in the past for the first time by Chang and Lundgren (1961). Bühler (1994) applied 18 to various geometries with reasonable results. This approach fails only close to the points where the boundaries are tangent to the magnetic field direction, where some special criterion should be adopted in order to limit the value of the effective wall conductivity. Roberts (1967) has shown that the error applying 18 is big only within a small radius of $O\left(M^{-1/3}\right)$ around the tangential point in the surface, and it extends for a radius of $O\left(M^{-2/3}\right)$ within the fluid; furthermore, the total flow rate carried is even of higher order.

It is interesting to point out that, in principle, it is possible correctly to describe the case in which there are several sheets of conducting materials with different properties surrounding the fluid domain, or the case of perfectly conducting walls with an electrical resistance between the wall and the fluid. The latter configuration was known in the past as 'insulating coating', and it has been studied for example by Bühler and Molokov (1994). In order to describe properly in CFX such a situation it is sufficient to change the electrical boundary condition at the external sides of the wall, from zero flux to a Dirichelet condition. In a similar way, it is possible to model an infinite lattice of rectangular ducts electrically coupled, by setting periodicity along the $\hat{\mathbf{y}}$ and $\hat{\mathbf{z}}$ directions. The model proposed can also be easily applied to pressure-driven MHD flow. In that case, the buoyancy term in the momentum equation 10 must be replaced by a constant forcing term. Once the flow field is known, the temperature distribution can be calculated solving an ordinary heat transfer problem. This approach is interesting for fusion self-cooled concepts.

This second way to model electrical boundary conditions using internal solvers has proved to be much more efficient than the first one described in the first part of the section; in particular, covergence speed is relatively high and only slightly influenced by the wall conductivity. There is no need of time-marching procedure or under-relaxation. About 5000÷20000 iterations are needed to get a converged solution. This is valid for the cases with internal heating, where the core currents are basically closed through the side layers and the side walls. The overall balance of the currents in this case is not very much affected by the Hartmann walls and layers. For the differentially heated cases, convergence is difficult to obtain for $c_w \lesssim M^{-1}$, where the closure of the currents through the Hartmann walls and layers is crucial for a converged solution. Here, the

low resolution along the field lines and the insufficient numerical accuracy are the main reasons for difficulties in convergence.

The cross section is resolved by a grid of $n_y \times n_z = 15 \times 250$ nodes for the calculations, with a non equispaced distribution of the grid points along $\hat{\mathbf{z}}$. Periodic boundary conditions are imposed along the axis direction and since fully developed flows are considered, only 3 grid points along the axis are sufficient to formulate the CFX model. For the simulations a CRAY J90 version of CFX has been used.

4 Results and discussion

4.1 Differentially heated duct

Let us consider differentially heated thermal boundary conditions at the side layers, for example $T = -1$ and $+1$ as boundary values. From Eq. 7 , the temperature profile is simply $T = z$, if no internal heat generation is present. In the plane purely hydrodynamic case, the velocity profile would be a third order parabola with a maximum value of $M^2/16$ adopting the present scales. Lorentz forces damp this profile, and the shape is completely modified. Fig.2 shows the velocity field computed for $M = 100$ and perfectly conducting walls ($c_w \to \infty$).

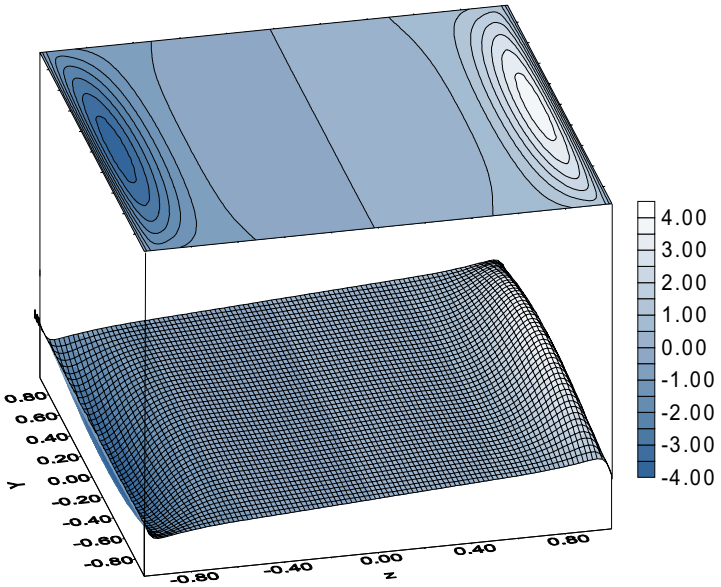

Figure 2: 2-D velocity distribution for a differentially heated duct with $T = z$, $M = 100$ and perfectly conducting walls. The flow exhibits velocity peaks in the side layers.

Of course, in this case the damping effect is more evident because the currents across the domain are the highest possible. In Fig.3, for the same case, a comparison is shown between the analytical and numerical solution in the plane $y = 0$.

The agreement is very good, because under these conditions asymptotic theory applies almost exactly, but it also proves the sufficiently high accuracy of CFX in describing such phenomena. It is possible to notice that velocity exhibits a linear profile in the centre of the core, where buoyancy is mainly balanced by Lorentz forces, and viscous effects are negligible. The slope is $\sim$1 as from the theory. The main feature of the profile in the side layer is the presence of a high velocity jet that is mainly governed by the current pattern and the viscous effects. A good explanation of such a jet can be found just considering that, from asymptotic theory, the correction to the core solution in the side layer is given by $u \sim \partial_z \phi_s$, where ϕ_s is the additional contribution of the side layer to the solution; therefore, the flow rate carried by the layer is $\dot{m} \sim \int \partial_z \phi_s dz \sim (\phi_{core} - \phi_{side-wall})$, which is $O(1)$. As already mentioned, it is well known that the thickness of the side

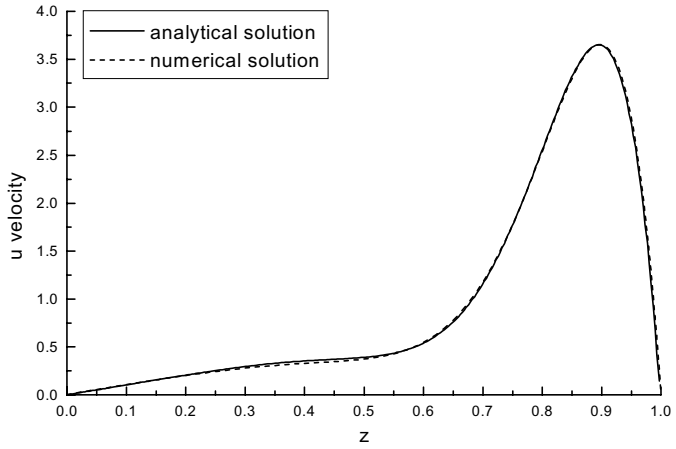

Figure 3: Comparison between analytical and numerical solutions, in the plane $y = 0$, for a differentially heated duct, with $T = z$, $M = 100$ and perfectly conducting walls. In this case the asymptotic theory applies almost exactly.

layer is $O(M^{-1/2})$, and thus the velocity in the jet must scale as $\sqrt{M}$. From these considerations it is easy to understand the potential profile shown in Fig. 4; here the gradient in the side layer actually sustain the velocity peak.

Fig. 5 shows the velocity profiles in the plane $y = 0$ for some other values of the wall conductivity and $M = 100$; the limiting case of perfectly insulating walls is also included. For the lower values of c_w the MHD damping effect is less evident, but the core part of the solution is still dominated by Lorentz forces, as it is possible to recognize by the linear behaviour. In the case of insulating walls, the slope is $\sim M$, as in the asymptotic analytical solution provided by Aleksandrova (1999), which refers to the work of Bojarevics (1994). No more jets are present for these limiting cases; in fact the core solution is simply corrected by viscous dissipation in the side layer in order to satisfy the no slip condition at the wall. This behaviour at the lower values of wall conductivity can be understood if we look at the currents normal to the walls shown in Fig.6. Here, the coordinate ζ_{wall} starts from $y = 0,\ z = -1$ and follows the walls. For the highest value of c_w shown in the picture, the currents leaving the side walls passes almost unchanged the side layers and close through the Hartmann wall and layer. For the lower values, the currents leaving the side wall, are progressively reducing, and are almost negligible for $c_w \lesssim 10^{-2}$. In these latter cases, the side layers becomes better conducting than the side walls and high current jets are now present in the layers, parallel to the side walls. Currents parallel to $\mathbf{B}$ do not interact with the magnetic field. Therefore, the electric magnetic forces in the side layers become negligible and viscous dissipation is dominant. Of course, this behaviour cannot be recovered by the asymptotic approach, that is valid for well conducting side walls. Fig. 7 shows the electrical potential distribution along the wall for some values of c_w and $M = 100$. From the Ohm's law 5 and the thin wall condition 17 it comes that the first derivative of these distributions are proportional by

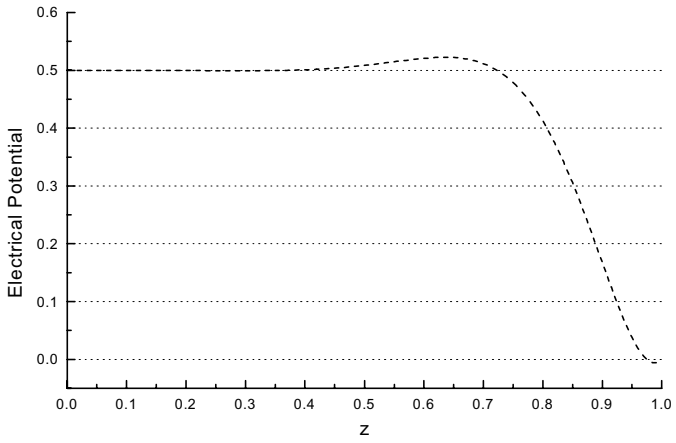

Figure 4: Potential distribution, in the plane $y = 0$, for a differentially heated duct, with $T = z$, $M = 100$ and perfectly conducting walls. The velocity jet in the side layer is actually sustained by the potential gradient.

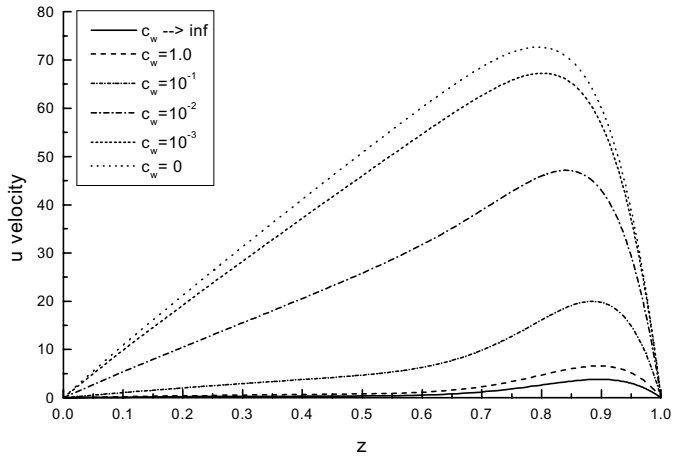

Figure 5: Velocity profiles, in the plane $y = 0$, for a differentially heated duct, with $T = z$, $M = 100$ for several values of the wall conductivity. For the limiting case of perfectly insulating walls and for the lower values of c_w the velocity jets are not present, and the linear core solution is corrected in the side layer only by viscosity.

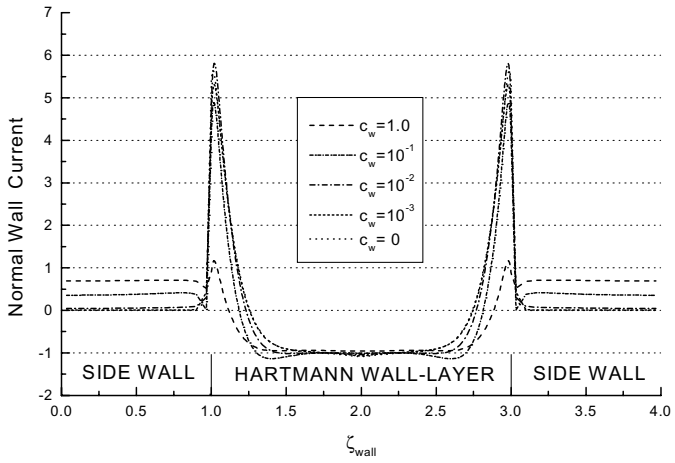

Figure 6: Normal wall currents for a differntially heated duct, with $T = z$, $M = 100$ for several values of the wall conductance ratio c_w. For good conducting walls currents leaving the side walls are basically totally closed via Hartmann wall-layer. For bad conducting walls, the side layers become better conducting than the side walls and high currents flow in the layers parallel to the walls before they enter the Hartmann walls near $\zeta_{wall} = 1$ or $\zeta_{wall} = 3$.

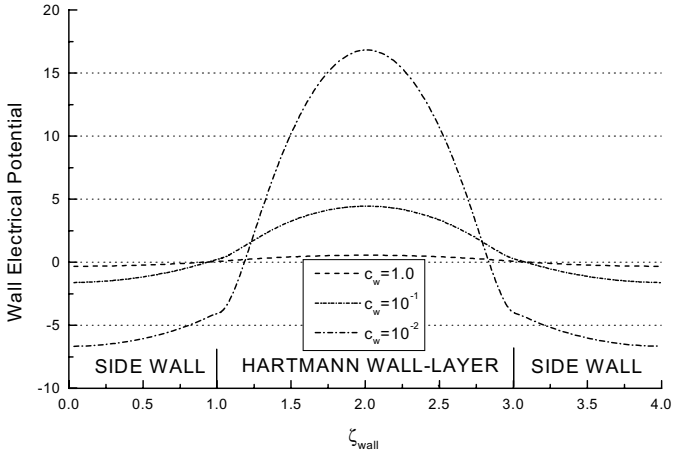

Figure 7: Potential distribution for a differentially heated duct, with $T = z$, $M = 100$ for some values of c_w. The first and the second derivatives, amplified by the local effective conductivity, give, respectively, the currents flowing within the walls, and the currents entering normally the walls.

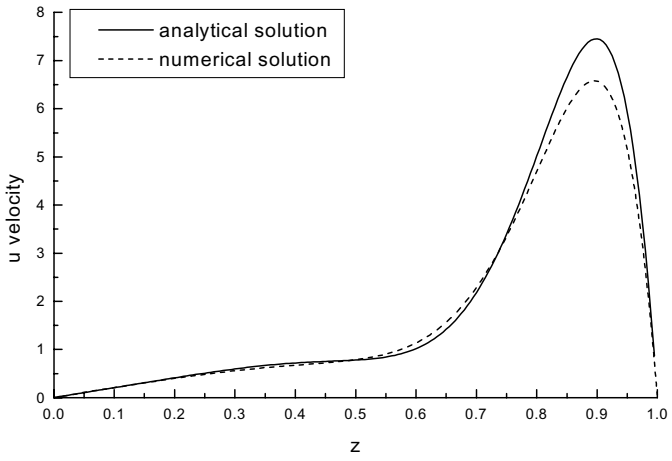

Figure 8: Comparison between analytical and numerical solutions, in the plane $y = 0$, for a differentially heated duct, with $T = z$, $M = 100$ and $c_w = 1$. The agreement is quite good in the core, while in the side layer the asymptotic approach doesn't apply exactly because relevant currents flow parallel to the wall within the side layer.

the local effective wall conductivity to the currents within the wall, while the second derivative is proportional to the currents entering normally the wall; thus it becomes clear that for bad conducting materials, currents interesting the side walls are very low.

The agreement between numerical and analytical results is also rather good for relatively high wall conductivities. For $M = 100$, $c_w = 1$, criterion 9 is satisfied, but the actual thickness of the side layer seems to be larger than $M^{-1/2}$ and currents are already present parallel to the walls.

Fig. 8 shows such a comparison in the plane $y = 0$. The agreement is good in the core, while the maximum value is not correctly predicted by the theory. Similar remarks hold for higher values of the Hartmann number M as shown in Fig. 9 for $M = 400$, $c_w = 1$.

Figures 10 and 11 show velocity profiles for a differentially heated duct with $T = z$ and higher values of the Hartmann number $M = 400$, $M = 1000$. It should be noticed that, also for this relatively high values of M, the velocity profile in the core is linear. This is valid also for the lower values of c_w and, as already observed previously in this section, this states that the Lorentz electro-magnetic forces steel play a major role in the core of the fluid domain.

4.2 Internally heated duct

If internal heat generation is present, the temperature profile established is parabolic. Therefore, in the purely hydrodynamic case, the flow goes up in the centre and down close to the left and right walls which are kept at $T = 0$, if all other walls are adiabatic. In order to satisfy the condition of zero net mass flux through the section, a dynamic

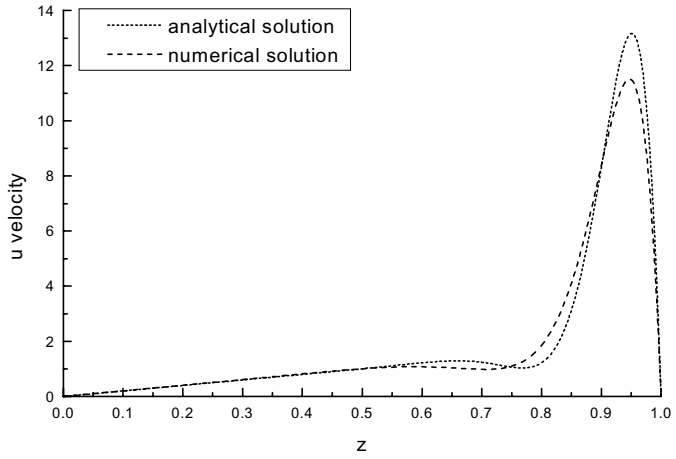

Figure 9: Comparison between analytical and numerical solutions, in the plane $y = 0$, for a differentially heated duct, with $T = z$, $M = 400$ and $c_w = 1$.

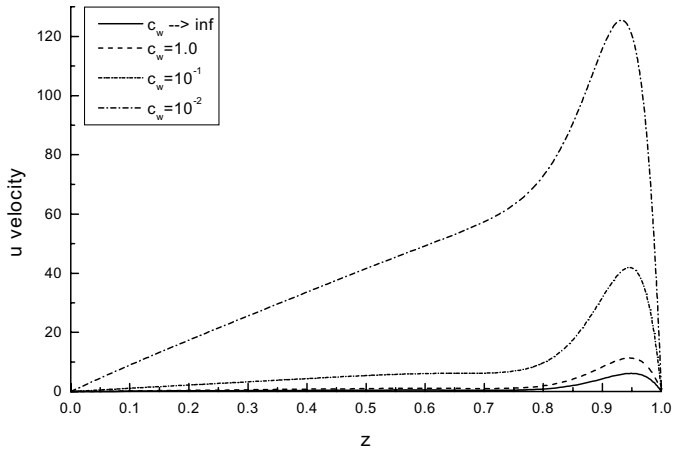

Figure 10: Velocity profiles, in the plane $y = 0$, for a differentially heated duct, with $T = z$, $M = 400$ for several values of the wall conductance ratio c_w. The limiting case of perfectly insulating walls is included

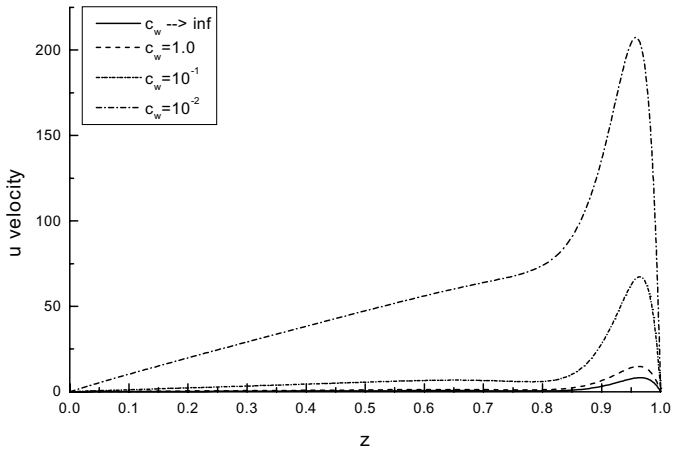

Figure 11: Velocity profiles, in the plane $y = 0$, for a differentially heated duct, with $T = z$, $M = 1000$ for several values of the wall conductance ratio c_w. The limiting case of perfectly insulating walls is included

compensative force in the momentum equation is needed to perform such simulations with internal heating. The velocity profile in a plane case would be a forth order parabola. The situation, of course, is very much modified by the presence of the magnetic field. The velocity profile is damped by Joule's dissipation as shown in Fig. 12 for perfectly conducting walls, $M = 100$, $Q = 1$, in the plane $y = 0$. High velocity jets are present again in the side layers, and the flow rate carried is of $O(1)$. Fig. 13 shows results for several values of wall conductivity, $M = 100$, $Q = 1$. As in the case of the differentially heated duct, and for similar reasons, flow jets are no more present when the conductivity of the wall decreases. In fact, the parabolic solution in the core is only corrected at the layers by viscous dissipation to satisfy no-slip at the wall. It is evident that the solution for $c_w = 10^{-3}$ is already very close to the limiting situation of perfectly insulating walls. This is not the case for higher values of the Hartmann number, as it is shown by Figs. 14 and 15. In these latter cases the conductance of the layers are relatively low, and a residual influence of the wall conductivity is still present above 10^{-3}. A comparison between solutions at different Hartmann numbers is given in Fig.16 for $c_w = 1$. The core solution is almost coincident in all cases and the thickness of the side boundary layer decreases as M increases. This is better shown by Fig.17, in which the side layer thickness δ_s is computed as the distance between the wall and the inflection points of velocity jets in Fig.16. The theoretical scaling of δ_s as $\delta_s \sim M^{-1/2}$ is fully confirmed by computations also for relatively low Hartmann number $M = 100$. It must be pointed out that this result is a consequence of the solution of the basic flow equations, without any additional hypotesis on the thickness of the side boundary layers. Similar remarks as in the previous section hold for the current patterns and their role in the fluid motion. High currents occur in the layers for the low conducting cases, as shown in Fig. 18 for $M = 1000$, $Q = 1$.

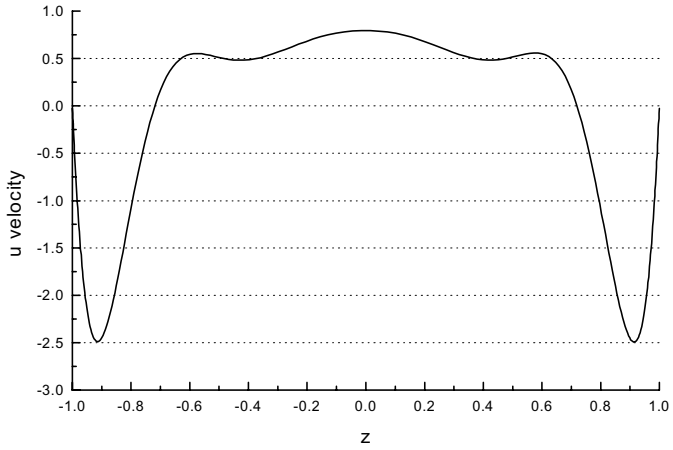

Figure 12: Velocity distribution in the plane $y = 0$, for an internally heated duct, with $Q = 1$ and $M = 100$. The flow is strongly damped in the core, while high velocity jets occur in the layers.

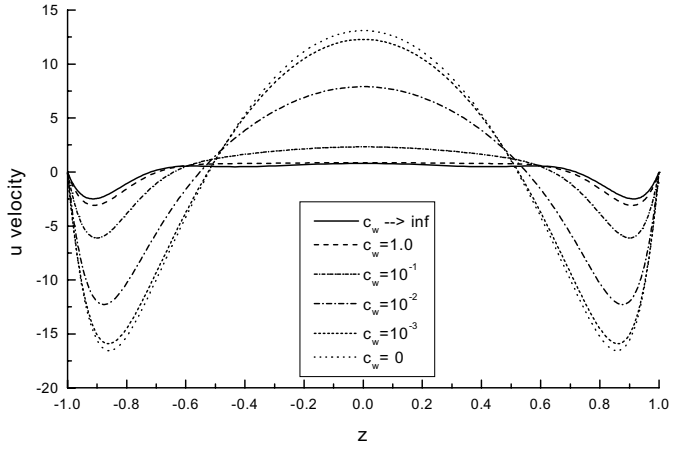

Figure 13: Velocity distributions in the plane $y = 0$, for an internally heated duct, with $Q = 1$ and $M = 100$ for several values of the wall conductance ratio c_w. The limiting cases of perfectly conducting and perfectly insulating walls are included.

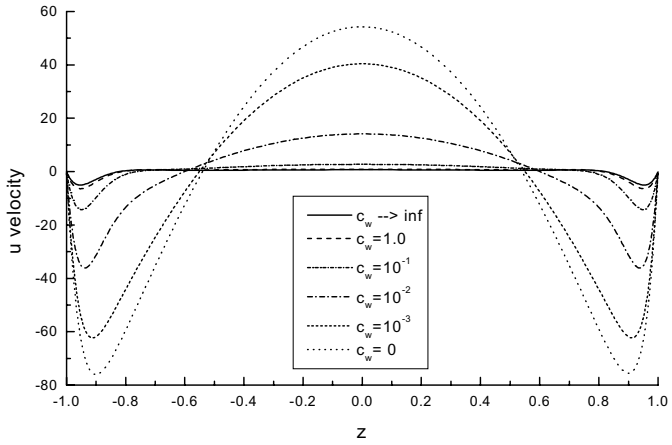

Figure 14: Velocity distributions in the plane $y = 0$, for an internally heated duct, with $Q = 1$ and $M = 400$ for several values of the wall conductivity c_w.

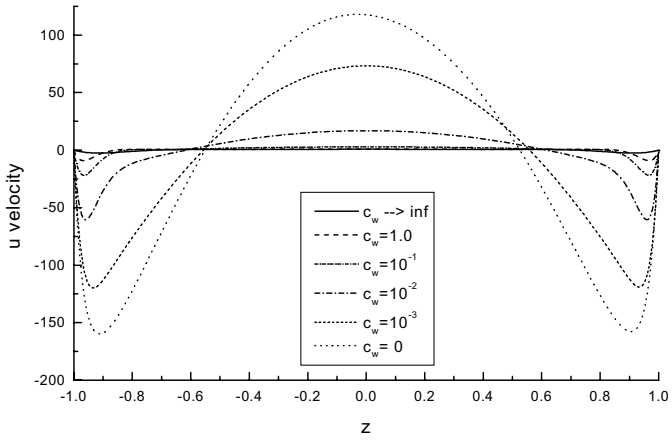

Figure 15: Velocity distributions in the plane $y = 0$, for an internally heated duct, with $Q = 1$ and $M = 1000$ for several values of the wall conductance ratio c_w. For these higher Hartmann numbers the solution obtained for $c_w = 10^{-3}$ is still far from the limiting case of perfectly insulating walls.

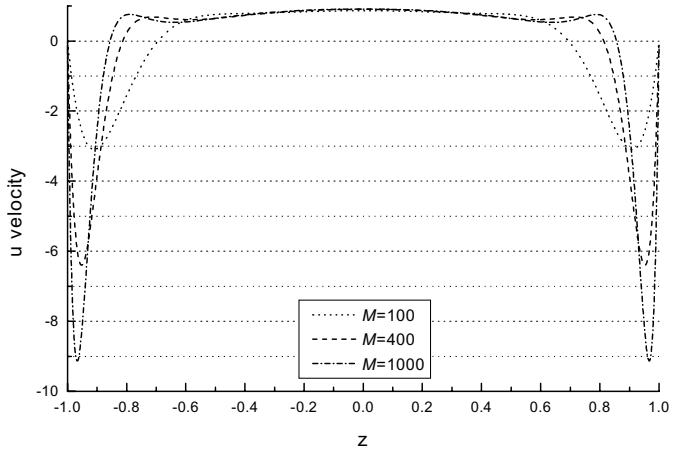

Figure 16: Comparison between numerical solutions in the plane $y = 0$, for an internally heated duct, with $Q = 1$, $c_w = 1$ and three different values of the Hartmann number. The solution in the core is almost independent of M, while the thickness of the side layer scales as $\sim M^{-1/2}$.

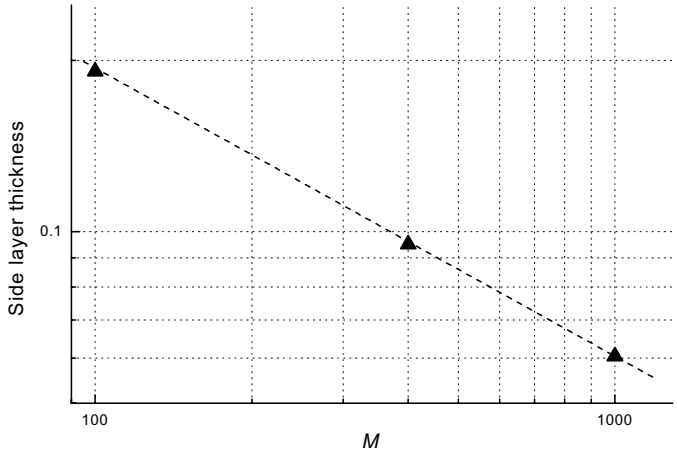

Figure 17: Comparison between numerical solutions in the plane $y = 0$, for an internally heated duct, with $Q = 1$, $c_w = 1$ and three different values of the Hartmann number. The thickness of the side layer is computed as the distance of the velocity inflection point from the wall. This thickness scales almost perfectly as $\sim M^{-1/2}$.

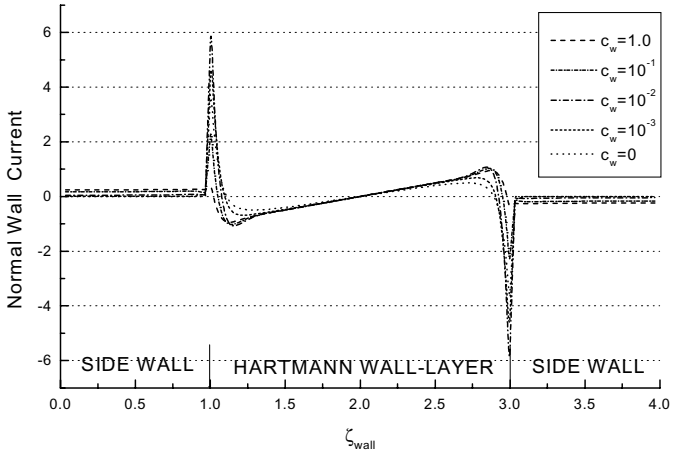

Figure 18: Currents occuring normally to the walls in an internally heated duct, with $Q = 1$, $M = 1000$ and several values of c_w. Like in the differentially heated duct, high currents flow in the side layers for bad conducting walls.

5 Conclusions

Numerical simulations of MHD buoyant-driven flow in a vertical square duct is presented. The CFX package has been used for all the calculations. The proper description of an MHD problem within the code is discussed, with particular reference to the Lorentz forces, the potential equation, and the electrical boundary conditions. The method presented is very general and allows, in principle, to treat practical configurations using body-fitted coordinates, with arbitrary electrical conductivity of the walls and also pressure-driven flows can be computed. It is possible also to study flows in different domains which are electrically coupled or configurations like 'insulating coatings'. Results in a wide range of wall conductivity are illustrated and compared with the asymptotic theory. The capability of CFX to describe accurately MHD phenomena has been shown by comparing numerical and analytical results in some asymptotic cases. The agreement is very good for well conducting walls and high velocity jets are correctly predicted in the side layer, while for the lower values of wall conductivity, numerical simulations provide high current density flowing in the side layer parallel to the side wall. This is reasonable because for such lower values of c_w, the layers become progressively better conducting than the walls, and for the limiting case of insulating walls the whole current is closed by side layers. The asymptotic theory is valid under the assumption of good conducting walls, and it cannot be used to predict flows at low c_w.

The MHD problem in CFX, in particular the equation for electric potential, is treated as an equivalent heat transfer problem in a medium at rest, using conducting solid walls in order to describe the electrical thin wall boundary condition. This is an efficient way to solve the problem within the CFX available apparatus. Another method is in fact proposed to couple the CFX solvers for the fluid domain with an external Poisson solver which provides a Dirichelet boundary condition for the electrical potential. With this latter method the convergence speed is much lower and a time-marching procedure must be adopted. Nevertheless, one can notice that the coupling between electrical potential and velocity field is of a similar nature of the better known pressure-velocity coupling. Therefore, probably it would be even more efficient to treat electrical potential as a second pressure using the same SIMPLE family algorithm for the velocity coupling. This is not possible at the moment with CFX, because the simple algorithm is available only for the pressure, and a second pressure cannot be actually defined.

References

Aleksandrova, S.: 1999, Natural convection in a rectangular cavity in a strong vertical magnetic field, Technical Report Transfer Document from MPhil/PhD to PhD, Coventry University M.I.S.

Ben Hadid, H. and Henri, D.: 1997, Numerical study of convection in a horizontal Bridgeman configuration under the action of a constant magnetic field. Part 2. three-dimensional flow, Journal of Fluid Mechanics **333**, 57–83.

Bojarevics, V.: 1994, Buoyancy driven flow and its stability in a horizontal rectangular channel with an arbitrary oriented transverse magnetic field, Technical report.

Bühler, L.: 1994, Magnetohydrodynamic flows in arbitrary geometries in strong, nonuniform magnetic fields.-a numerical code for the design of fusion reactor blankets, Fusion Technology **27**, 3–24.

Bühler, L.: 1998, Laminar buoyant magnetohydrodynamic flow in vertical rectangular ducts, Physics of Fluids **10**(1), 223–236.

Bühler, L. and Molokov, S.: 1994, Magnetohydrodynamic flows in ducts with insulating coatings, Magnetohydrodynamics **30**(4), 439–447.

Chang, C. and Lundgren, S.: 1961, Duct flow in magnetohydrodynamics, ZAMP **XII**, 100–114.

Leboucher, L.: 1999, Monotone scheme and boundary conditions for finite volume simulation of magnetohydrodynamic internal flows at high Hartmann number, Journal of Computational Physics **150**, 181–198.

Mößner, R. and Gerbeth, G.: 1999, Buoyant melt flows under the influence od steady and rotating magnetic fields, Journal of Crystal Growth **197**, 341–354.

Mück, B.: 1998, Numerische Untersuchung von Strömumgen in Kanälen mit Versperrungen unter dem Einfluß von Magnetfeldern, Technical Report FZKA 6292, Forschungszentrum Karlsruhe.

Reimann, J., Benamati, G. and Moreau, R.: 1996, MHD issues of the European self-cooled and water-cooled 83Pb-17Li blankets, in C. Varandas and F. Serra (eds), Fusion Technology 1996, Proceedings of the 19th Symposium on Fusion Technology, Lisbon, Portugal, 16-20 September, North-Holland, pp. 1527–1530.

Roberts, P. H.: 1967, Singularities of Hartmann layers, Proceedings of the Royal Society of London **300**(A), 94–107.

Sterl, A.: 1990, Numerical simulation of liquid-metal MHD flows in rectangular ducts, Journal of Fluid Mechanics **216**, 161–191.

Walker, J. S.: 1981, Magnetohydrodynamic flows in rectangular ducts with thin conducting walls, Journal de Méchanique **20**(1), 79–112.